Accepted Manuscript

Optical, structural and electric characterization of stacked Hf-based and silicon nitride dielectrics

L. Khomenkova, P. Normand, F. Gourbilleau, A. Slaoui, C. Bonafos

Please cite this article as: L. Khomenkova, P. Normand, F. Gourbilleau, A. Slaoui, C. Bonafos, Optical, structural and electric characterization of stacked Hf-based and silicon nitride dielectrics, *Thin Solid Films* (2016), doi: 10.1016/j.tsf.2016.04.036

Optical, structural and electric characterization of stacked Hf-based and silicon nitride dielectrics

L. Khomenkova[1,2,3,*], P. Normand[4], F. Gourbilleau[3], A. Slaoui[5], C. Bonafos[2]

[1] V.Lashkaryov Institute of Semiconductor Physics of NASU, 45 Pr.Nauky, 03028 Kyiv, Ukraine

[2] CEMES/CNRS, Université de Toulouse, 29 rue J. Marvig 31055 Toulouse Cedex 4, France

[3] CIMAP, CEA/CNRS/ENSICAEN/Unicaen, 6 Blvd Marechal Juin, 14050 Caen Cedex 4, France

[4] INN / NCSR Demokritos, 15310 Aghia Paraskevi, P.O.Box 60228, Athens, Greece

[5] ICube, 23 rue du Loess 67037 Strasbourg, France

[*] Corresponding author: L. Khomenkova,

e-mail: khomen@ukr.net, phone +38-044-5255775; fax: +38-044-5258243

Abstract. High-k stacked dielectric structures were fabricated by a combination of RF magnetron sputtering and plasma-enhanced chemical vapor deposition. Their structural properties were studied versus deposition and annealing conditions by means of attenuated total reflection and high-resolution transmission electron microscopy techniques. All samples demonstrated smoothed surface (with a roughness below 1 nm) and abrupt interfaces between the different stacked layers. No crystallization of Hf-based layers was observed after annealing at 800°C for 30 min, demonstrating their amorphous nature and phase stability upon annealing. Uniform capacitance-voltage characteristics were measured along the wafers for all stacks. Besides, after round-voltage sweep they demonstrate significant flat-band voltage hysteresis due to charging of the stack caused by carrier injection from the substrate. These phenomena were found to be more pronounced for the stacks with pure HfO_2 layers. The stacked structures were implemented for the formation of Ge nanocrystals by means of ion implantation followed by the thermal treatment mentioned above. It was found that the spatial distribution of Ge crystallites in stacked dielectrics affects significantly their electrical properties including the trapping of charge.

Keywords: High-k dielectrics; RF magnetron sputtering; Plasma-enhanced chemical vapor deposition; Memory effect.

1. Introduction

The increasing market for portable electronic products (mobile phones, digital cameras, external data storage devices, players etc.) stimulated the development of nonvolatile memory (NVM) production. Among various NVM architectures, flash memory has out run other competitors due to its full process compatibility with CMOS technology and superior performance [1]. However, conventional floating gate structures have already faced a limit due to the aggressive scaling trend in the vertical dimension.

The stacked dielectrics such as MNOS (metal-nitride-oxide-silicon), SONOS (silicon-oxide-nitride-oxide-silicon), MONOS (metal-oxide-nitride-oxide-silicon), MOHOS (metal–oxide–high-dielectric–oxide–semiconductor) etc. were considered as promising alternatives for next-generation flash memory applications due to layer's scalability, process simplicity, power economy, operation versatility, and radiation hardness [2]. Nevertheless, the continued minimization of NVM structures forces an application of high-k dielectrics instead conventional silicon nitride trapping layer. For instance, pure and/or Al-doped HfO_2 layers were stacked in MONOS-like structures, demonstrating better charge trapping parameters for sufficient density trap states and deep trap energy level to achieve longer retention time [3,4]. The application of stacked $HfO_2/SiON/SiN$ structures as charge trap node in junction-less memory structures was demonstrated to achieve high programming speed and good endurance [5].

There are many technological approaches used for the production of high-k dielectric films such as atomic layer deposition (ALD) [6,7], different chemical vapor deposition (CVD) techniques [8-10], sol-gel process [11,12], pulsed laser deposition [13,14] etc. However, despite its flexibility radio-frequency magnetron sputtering (RF-MS) was not often addressed [15,16].

Recently we have shown the simplicity and utility of the RF-MS approach for the production of fully Hf-based NVM structures with large memory windows and enhanced dielectric properties in one deposition run [17]. Besides, we have demonstrated that this approach can be used to form Si nanocrystals (Si-ncs) in Hf-based host via phase separation process [18,19] that required a lower thermal budget compared to the formation of Si-ncs in SiO_2 or Al_2O_3 matrix [20]. It was shown also that Ge-ncs can be produced in Hf-based or Zr-based dielectrics at 600-650°C for 30 s depending on Ge content [21,22]. These annealing conditions are "softer" than those used for Ge-ncs formation in Si_3N_4 films after Ge ion implantation (800-900°C for 15 min) [23].

It was considered that Hf-based dielectrics suffer from their poor thermal stability as well as from the formation of a SiO_2 interfacial layer either during the deposition process or upon thermal treatment [24,25]. To solve these problems, the use of silicon nitride interlayer or the doping of HfO_2 with silicon were considered as the most promising [16,26].

This work concerns the elaboration of high-k dielectric structures based on the combination of Hf-based and SiN$_x$ materials grown by RF-MS and plasma-enhanced CVD (PECVD) approaches aiming at the achievement of good-quality interfaces between the various dielectric layers and smooth surface of the stacks. The interrelation of their structural and electrical properties was investigated as a function of deposition and post-annealing conditions for the pinpointing of optimal device architectures. Besides, the stacks were implanted with germanium followed by thermal treatment aiming at the formation of Ge-ncs and the investigation of their properties for possible application in memory devices.

2. Experimental details and methods

2.1. Fabrication of dielectric layers and complex stacked structures. The stacks were grown on 2-in. B-doped, (100) oriented Si wafer with a resistivity of 15 Ω·cm (Sil'tronix S.T.). Prior deposition, Si wafer was subjected to standard RCA cleaning process, dipped in a diluted hydrofluoric solution (10%) for 10 s to remove thermal SiO$_2$ layer from the surface. This procedure allowed only hydrogen termination of the Si wafer surface to be reached. After drying with pure N$_2$ flow, the wafers were immediately transferred into the "load-lock" chamber of the deposition unit.

Single HfO$_2$ and Hf silicate layers were grown at 100°C by "bottom-up" RF-MS sputtering of pure HfO$_2$ (99.9%) and mixed Si-HfO$_2$ targets, respectively, in pure Ar plasma. To produce Hf silicate layers, pure HfO$_2$ target was topped with calibrated Si pellets. They covered about 6% or 12% of target surface allowed to achieve Hf$_{0.27}$Si$_{0.05}$O$_{0.68}$ or Hf$_{0.17}$Si$_{0.25}$O$_{0.58}$ compositions, respectively. The RF power applied on HfO$_2$ cathode was 0.74W/cm^2 for all depositions.

Single Si nitride layers were produced both RF-MS and PECVD methods. In the former case, the nitride layer of the SiN$_{0.8}$ composition was obtained by the sputtering of a pure Si target in Ar-N$_2$ mixed plasma at 500°C, whereas PECVD layers with SiN$_{1.33}$ stoichiometry were grown from a SiH$_4$-N$_2$ mixture at 350°C. More details about these techniques can be found in [15,16,23]. The deposition time for single Hf-based layers and complex stacks was chosen to achieve an equivalent oxide thickness (EOT) of in the range 2-3 nm.

After deposition of the above dielectric films, an additional 12-nm-thick Si nitride layer was grown either by RF-MS or PECVD methods. Then each wafer was cut on 2 parts. One of them was implanted with ^{74}Ge$^+$ ions using GeH$_4$ gas as a source. The implantation energy and the dose were 5 keV and 1.5×10^{16} at/cm^2, respectively. All the samples were annealed at 800°C for 30 min in a conventional horizontal furnace in pure dry nitrogen flux. The furnace was heated up to 800°C without samples. The samples were placed on horizontal holder in cold load-lock, pumped and purged with nitrogen flow at 48 sccm during 5 min, and then passed in within 15 s into the hot zone of the furnace with continuous nitrogen flow. After annealing (30 min in the present study) the

samples were removed from the furnace within 15 s and cooled down to room temperature in nitrogen ambient. For Ge-implanted samples such treatment allows the formation of Ge crystallites [23].

The architecture of all the samples investigated is presented in Table I. For easier recognition of the different parts of the same wafer submitted to different treatment (annealing, implantation), the samples were re-numerated as follows. "R1" marks the as-deposited and unimplanted sample, while "R2" marks the unimplanted and annealed at 800°C for 30 min samples. The "Ge3" mark is used for the samples submitted to Ge implantation and annealing at 800°C for 30 min.

2.2. Experimental methods. The combination of non-destructive methods allows information about microstructural and optical properties of the films. Infrared attenuated total reflectance (ATR-FTIR), was used to provide information about the structure and chemical composition of the films. The ATR-FTIR spectra were measured in the range 600-4000 cm^{-1} by means of a 60° Ge Smart Ark accessory inserted in a Nicolet Nexus spectrometer.

The analysis of the structural properties was completed by high-resolution transmission electron microcopy (TEM) observation. Cross-sectional specimens were prepared by the standard procedure involving grinding, dimpling and Ar^+ ion beam thinning until electron transparency. The samples were examined using a FEI Tecnai microscope operating at 200 keV equipped with a field emission gun and a spherical aberration corrector.

For electrical characterization, Al was deposited by thermal evaporation on the as-deposited and annealed samples to form top electrodes of 100×100 μm^2 using photolithography and the back side contact. Capacitance-voltage (C-V) characteristics of the so-formed metal-insulator-semiconductor (MIS) capacitors were measured at different frequencies using a HP 4192A Impedance Analyzer.

3. Results and discussion

3.1. ATR-FTIR spectra of as-deposited and annealed samples. Among nondestructive methods to study thin films, ATR technique holds an important place, since it allows very thin layers to be analyzed. Unfortunately, referenced ATR data for Hf silicates are not so numerous. The only known data are those regarding the monoclinic HfO_2 phase, while for tetragonal and cubic phases of HfO_2 and, moreover, for $HfSiO_4$ they are not available in the case of ultra-thin films.

There are few reports on traditional FTIR experiments for Hf silicate films [26,28] that considered Hf silicates as a solid solution consisted of HfO_2 and SiO_2 unit cells, i.e. as a $(HfO_2)_x(SiO_2)_{1-x}$. Recently, we have shown that the interpretation of experimental ATR data for Hf

silicate materials can be based on the comparison of ATR spectra obtained for amorphous SiO_2 and HfO_2 and their transformation due to increase of high-k material contribution [16].

The SiO_2 films thicker than 50 nm demonstrate several vibration bands in the 600-1300 cm^{-1} spectral range caused by motion of oxygen atoms. They are centered at about 1076 cm^{-1} (transverse optical phonon, TO_3) and 1256 cm^{-1} (longitude optical phonon, LO_3), at 1160 cm^{-1} (TO_4) and 1200 cm^{-1} (LO_4), at 810 cm^{-1} (TO_2) and 820 cm^{-1} (LO_2) [29,30]. The decrease of the SiO_2 thickness to 10 nm leads to the spectral shift of all vibration bands towards the lower wavenumbers. For LO_3 and TO_3 it can reach about 25-30 cm^{-1} [31], being accompanied to the decrease of the contribution of TO_4-LO_4 phonons [30]. This transformation of FTIR spectra with the thickness scaling brings some difficulty in the recognition of different vibration bands due to their significant overlapping. Moreover, the appearance of LO_3 Si-O phonon is usually reported as a signature of the formation of Si/SiO_2 interface [29]. Besides, the coordination number of Hf ions can also change versus Hf content in the silicate [16]. All these facts will result not only in the shift of main Si-O-Si band towards the lower wavenumbers due to the formation of Si-O-Hf bonds, but also an appearance of Hf-O vibrations themselves in 450-800 cm^{-1} spectral range [15,19,28,32].

Usually, the simultaneous appearance of the 770-780 cm^{-1} and 670-680 cm^{-1} vibration bands in FTIR spectra of Hf-based materials is considered as a signature of monoclinic HfO_2 phase [15,33], whereas the vibrations of random Si-O-Hf bonding can be seen in 900-1020 cm^{-1} spectral range being centered at ~970 cm^{-1} [34]. In the case of Si nitride materials the main Si-N vibrations can be detected in the 700-1100 cm^{-1}, demonstrating TO and LO phonons at about 840 cm^{-1} and 1080 cm^{-1} respectively [35,36].

The ATR-FTIR spectra of the as-deposited Hf-based layers and stacked structures grown by RF-MS approach are shown in Fig.1. The pure HfO_2 layer (sample A-R1) shows the presence of the characteristic Hf-O band located at ~720 cm^{-1}. No band peaking at 770-780 cm^{-1} was observed that testifies to the amorphous nature of HfO_2 layer. However, for this sample two vibration bands centered at ~920 cm^{-1} and ~1100 cm^{-1} can be seen (Fig.1a, curve 1). The former can be caused by Si-O-Hf vibrations [16] while the latter can originate either from Si-O-Si [16] or Si-O-Hf [29,32] bonds. Since the deposition of HfO_2 layers on Si substrate is usually accompanied by the appearance of SiO_2 IL, the band at ~1100 cm^{-1} can originate from the Si-O bonds formed within SiO_2 layer at the SiO_2-IL/Si interface, whereas Si-O-Hf bonds can construct at the SiO_2-IL/HfO_2 interface. This assumption agrees with the data of Ref. [15].

The spectrum of the B-R1 sample demonstrates two main bands localized at about 1100 cm^{-1} and 750 cm^{-1} with a shoulder-like feature at about 880-900 cm^{-1} (Fig.1a, curve 2). Since the $SiN_{0.8}$ layer was grown on H-terminated Si substrate, it is hardly believed that the band at about 1100 cm^{-1} can be caused by the formation of SiO_2 IL. Most probably it can be attributed to the vibration of

bonding groups involving Si, O, N, and Hf, which may be formed at the SiN/HfO_2 interface in small concentration. The band peaked at 750 cm^{-1} originates from Hf-O vibrations whereas the shoulder-like feature is due to overlapping of Si-N (peaking usually at 844-860 cm^{-1}) and Si-O-Hf bands. The comparison of ATR spectra of the $SiN_{0.8}/HfO_2$ (sample B-R1) and the $SiN_{0.8}/HfO_2/SiN_{0.8}$ structure (sample C-R1) shows that the presence of top $SiN_{0.8}$ layer causes the increase of the contribution of the band peaked at ~850 cm^{-1} (Fig.1a, curve 3).

The spectra of Hf silicate layers (used in sample D-R1 (curve 4) and sample E-R1 (curve 5)) demonstrate similar vibration bands in the 900-1200 cm^{-1} spectral range due-to Si-O-Hf bonds. However, for the film with higher Hf content (sample E-R1), the Hf-O related band is also observed in 600-850 cm^{-1} (curve 5). The featureless shape of this band is an evidence of the amorphous nature of this layer.

Annealing of the samples at 800°C for 30 min in N_2 flow results in the transformation of the ATR spectra (Fig.1,b). For the samples A-R2 (curve 1), B-R2 (curve 2) and C-R2 (curve 3), the appearance of LO_3 Si-O phonon peaked at ~1240 cm^{-1} testifies to the reconstruction of Si-O bonds towards the configuration observed for stoichiometric SiO_2 unit cell [16,34]. Besides, peak position of the Hf-O band shifts towards the lower wavenumbers. No additional Hf-O band at about 770 cm^{-1} was appeared that confirmed the amorphous nature of the Hf-based layer in the structures.

For the samples contained Hf silicate layers (samples D-R2 (curve 4) and E-R2 (curve 5)), annealing causes the transformation of Si-O-Hf network via the variation of the angles and lengths of the Si-O and Hf-O bonds and does not lead to significant phase separation [16,19].

The ATR spectrum of the B-R2 sample, besides the peak at ~1240 cm^{-1}, reveals an additional peak at ~1160 cm^{-1} (Fig.1b, curve 2). The appearance of these both bands can be explained by the reconstruction of Si-N bonds [35,36] as well as by the formation of Si-O bonds. However, the location of the latter cannot be clearly distinguished from the ATR spectra.

It is worth to note also that the ATR spectrum of the sample C-R2 shows slight transformation after annealing (Fig.1b, curve 3). The contribution of the Hf-O vibrations become more pronounced in the 600-800 cm^{-1} spectral range, but the featureless shape of this band confirms the amorphous HfO_2 nature. This means that this stacked structure is thermally stable until 800°C annealing. Along with this, the appearance of the peak at about 1240 cm^{-1} can be assigned to the Si-O bonds similar to the case of the D-R2 sample. The shape of ATR spectrum of sample F-R1 and its transformation after annealing (sample F-R2) were found to be similar to those of sample D-R1 and D-R2, respectively. A slight higher contribution of Si-N vibration bands in the spectra for samples F was detected (not shown here).

3.2. HR-TEM observation of the samples. HR-TEM observation was performed for all the samples described above. Earlier we have demonstrated that as-deposited samples (whatever the deposition approach) are homogeneous and smooth enough [15,16,18,23]. For the pure HfO_2 layers grown on Si substrate, SiO_2 interfacial layers (IL) thinner than 1 nm were observed. Other layers and structures did not show the formation of such SiO_2 IL. As-deposited samples grown by either RF-MS approach or by combination of RF-MS and PECVD techniques showed similar structural properties. The deposition of top $SiN_{1.33}$ layer by PECVD (when it was required) did not modify the structure of the underlying layers.

Figure 3 represents the HR-TEM images of the annealed samples. All the samples show smoothed surface (with the roughness below 1 nm) and abrupt interfaces between different stacked layers. No crystallization of Hf-based layers was observed for all structures. This means that neither the formation of grain boundaries in HfO_2 layers nor phase separation in Hf silicate ones occurred upon annealing at 800°C during 30 min. Besides, a good interface quality was also observed for the structures produced by combination of RF-MS and PECVD methods (Fig.2,a,b,d) offering good compatibility of both processes for device fabrication.

The formation of SiO_2 IL was observed only for the stacks with pure HfO_2 layers (sample A, Fig.2,a). The comparison of the stacks with the $SiN_{0.8}$ layer separating Hf-based layer from Si substrate in the samples B-R2, C-R2 and D-R2 (Fig.2,b-d) showed that the bottom $SiN_{0.8}$ layer prevents the development of SiO_2 IL for the structures with pure HfO_2 layer (samples B-R2 and C-R2, Fig.2c,d). The comparison of HR-TEM images with corresponding ATR-FTIR spectra allows assuming that the appearance of Si-O vibration band peaked at about 1240 cm^{-1} is due to either the reconstruction of Si-O bonds in Hf silicate layers (sample D-R2) or the formation of Si-O bonds at $SiN_{0.8}$/HfO_2 interface (samples B-R2 and C-R2). This fact showed that produced stacked structures will keep their high permittivity after processing that can be used for further vertical scaling of similar structures. The TEM study of the samples E-R2 and F-R2 revealed that their TEM images were very similar to that of sample D-R2 (not shown here).

The samples with $SiN_{1.33}$ top layer implanted with Ge and submitted to the annealing at 800°C (sample A-Ge3), showed the appearance and crystallization of numerous Ge-ncs (Fig.2a). The position of the formed Ge-ncs is in good agreement with the projected range and width of the low energy implanted profile predicted by TRIDYN for such samples. The Ge diffusion after annealing is limited here due to the low thermal budget used for Ge-ncs nucleation. It is worth to note that no Ge-ncs were observed in the top $SiN_{0.8}$ layer after such treatment (not shown here).

3.3. Electrical properties of the structures. High-frequency (100kHz-1MHz) C-V characteristics were measured for all samples. Single sweep measurements were first carried out along the

samples. The distance from capacitor to capacitor was about 3 mm (Fig. 3a-b). In most cases uniform C-V curves were obtained, so indicating a good uniformity in flat-band voltage and equivalent oxide thickness along the samples. No substantial difference in C-V data under light and dark conditions was observed.

Comparison of the C-V single sweeps for the different structures (Fig.3c) shows that the samples A-R2, C-R2 and D-R2 exhibit sharp C-V transition from the depletion to the accumulation regime. At the same time, the C-V curves of the samples B-R2, E-R2 or F-R2 suffer from a significant shift towards negative bias values that can be explained by the presence of a high amount of positive charge trapped in the stack.

Forward and backward C-V sweeps were registered for the samples A-R2, D-R2 and B-R2 (Fig.4), E-R2 and F-R2 (not shown here). Strong hysteresis phenomena were detected for the samples A-R2 (Fig.4a) and D-R2 (Fig.4b). These memory effects, depicted as flat-band voltage shifts in Fig. 4c, relate to both electron and hole injection from the substrate for the sample A-R2, while they are mainly caused by electron injection from the substrate in the case of the sample D-R2; a trait indicating a larger energy barrier for hole injection for the latter sample compared to the former. The charging effect was found to be uniform from capacitor to capacitor under light conditions. Only slight variations in the injection efficiency of minority carriers (electrons) were found under dark conditions.

Preliminary charge retention measurements have been performed at room temperature after application of a +6V gate voltage stress for 10s. Two charge-loss regimes were observed. A regime where a significant part of the injected charge (~30% for sample D-R2 and 60% for sample A-R2) is rapidly lost within the first 100s, and a second regime during which the flat-band voltage shift decreases linearly with the logarithm of the waiting time (see Fig. 4d). From the logarithmic time dependence of the charge loss, flat-band voltage shifts of about 0.2 (D-R2) and 0.1V (A-R2) are estimated for a 10-year waiting time. The two above regimes suggest two different charge-loss processes but more investigations are needed to draw safe conclusions on the leakage paths and the nature of the associated mechanisms.

C-V hysteresis was also observed for the sample B-R2 (Fig.5a), whereas no (or negligible) charge trapping was detected for the sample C-R2 (Fig.5b). These two samples differ in the stoichiometry of the top Si nitride layer. Stoichiometric $SiN_{1.33}$ (former case) is known to demonstrate good charge trapping characteristics [2,3,32,36]. Thus, one can assume that for the structures with top $SiN_{1.33}$ layer, the latter can contribute significantly to the hysteresis effect. Besides, Hf-silicate layer can also participate to charge trapping as it was shown earlier [17]. It is worth to note that the triple stacked samples demonstrated also good reproducibility in C-V characteristics from capacitor to capacitor.

C-V measurements of the samples implanted with Ge and submitted to annealing at 800°C (see Fig.5c) revealed the vanishing of the strong hysteresis phenomenon previously reported for the non-Ge-implanted sample (Fig.4a). Similar C-V data were obtained for most samples with embedded Ge-ncs. The comparison of their structural and electrical properties (Figs.3-5) allowed assuming that the lateral and vertical spatial distribution of Ge-ncs can be responsible for the disappearance of the memory effects. However, this effect requires further investigations and additional studies are ongoing to draw safe conclusions regarding the location and the retention time of the trapped charge.

4. Conclusions

Stacked dielectrics were fabricated by combination of RF magnetron sputtering and PECVD approaches. All the stacked samples demonstrate good interface and surface roughness quality after thermal treatment at 800°C for 30 min in N_2 flow. Amorphous nature and stable phase composition were observed for pure HfO_2 and Hf silicate layers after annealing. Significant charging effects caused by carriers' injection from the substrate and further trapping were observed for the stacks with a top Si nitride layer grown by PECVD. No substantial memory phenomenon was observed when Ge nanocrystals were formed in the top Si nitride layer. Such a concern may be related to the spatial distribution of the Ge nanocrystals within the dielectric stacks but more research is needed to confirm this point.

Acknowledgment

References

[1] S. Gerardin, A. Paccagnella, Present and Future Non-Volatile Memories for Space, IEEE Trans. Nucl. Sci., 57 (2010) 3016-3039.

[2] M. L. French, C. Y. Chen, H. Sathianathan, M. H. White, Design and scaling of a SONOS multidielectric device for nonvolatile memory applications, IEEE Trans. Compon., Packag., Manuf. Technol A, 17 (1994) 390-397.

[3] X. Wang, J. Liu, W. Bai, D. L. Kwong, A novel MONOS-type nonvolatile memory using high-κ dielectrics for improved data retention and programming speed, IEEE Trans. Electron Devices, 51 (2004) 597-602.

[4] M. S. Joo, B. J. Cho, C. C. Yeo, D. S. H. Chan, S. J. Whoang, S. Matthew, L. K. Bera, N. Bala, D. L. Kwong, Formation of hafnium-aluminum-oxide gate dielectric using single cocktail liquid source in MOCVD process, IEEE Trans. Electron Devices, 50 (2003) 2088-2094.

[5] H.-K. Fang, K.-S. Chang-Liao, C.-Y. Chen, H.-W. Ho, Effects of HfO_2/SiON/SiN stacked trapping layer on operation characteristics of poly-Si flash memory devices, Microel. Eng. 138 (2015) 107-110.

[6] H.K. Kim, I-H. Yu, J.H. Lee, Ch. S. Hwang, Interfacial Dead-Layer Effects in Hf-Silicate Films with Pt or RuO_2 Gates, ACS Appl. Mater. Inter. 5 (2013) 6769-6772.

[7] R. Chau, S. Datta, M. Doczy, B. Doyle, J. Kavalieros, M. Metz, High-k/metal-gate stack and its MOSFET characteristics, IEEE Electron Device Lett. 25 (2004) 408-410.

[8] M.S. Kim, Y.D. Ko, M. Yun, J.H. Hong, M.C. Jeong, J.M. Myoung, I. Yun, Characterization and process effects of HfO_2 thin films grown by metal-organic molecular beam epitaxy, Mater. Sci. Eng. B 123 (2005) 20-30.

[9] A.C. Jones, P.R. Chalker, Some recent developments in the chemical vapour deposition of electroceramic oxides, J. Phys. D: Appl. Phys. 36 (2003) R80-R95.

[10] M. Lemberger, A. Paskaleva, S. Zürcher, A.J. Bauer, L. Frey, H. Ryssel, Electrical properties of hafnium silicate films obtained from a single-source MOCVD precursor, Microel. Reliab. 45 (2005) 819-822.

[11] T. Nishide, S. Honda, M. Matsuura, M. Ide, Surface, structural and optical properties of sol-gel derived HfO_2 films, Thin Solid Films 371 (2000) 61-65.

[12] M.G. Blanchin, B. Canut, Y. Lambert, V.S. Teodorescu, A. Barau, M. Zaharescu, Structure and dielectric properties of HfO_2 films prepared by a sol–gel route, J. Sol–Gel Sci. Technol. 47 (2008) 165-172.

[13] H. Hu, C.X. Zhu, Y.F. Lu, Y.H. Wu, T. Liew, M.F. Li, B.J. Cho, W.K. Choi, N. Yakovlev, Physical and electrical characterization of HfO_2 metal–insulator–metal capacitors for Si analog circuit applications, J. Appl. Phys. 94 (2003) 551-557.

[14] S.S. Hullavarad, D.E. Pugel, E.B. Jones, R.D. Vispute, T. Venkatesan, Low Leakage Current Transport and High Breakdown Strength of Pulsed Laser Deposited HfO_2/SiC Metal-Insulator-Semiconductor Device Structures, J. Electron. Mater. 36 (2007) 648-653.

[15] L. Khomenkova, C. Dufour, P.-E. Coulon, C. Bonafos, F. Gourbilleau, High-k Hf-based layers grown by RF magnetron sputtering, Nanotechnology 21 (2010) 095704.

[16] L. Khomenkova, X. Portier, J. Cardin, F. Gourbilleau, Thermal stability of high-k Si-rich HfO_2 layers grown by RF magnetron sputtering, Nanotechnology 21 (2010) 285707.

[17] L. Khomenkova, X. Portier, A. Slaoui, F. Gourbilleau, Charge Trapping in Hafnium Silicate Films with Modulated Composition and Enhanced Permittivity, Adv. Mat. Res., 854 (2014) 125-133.

[18] E. Talbot, M. Roussel, L. Khomenkova, F. Gourbilleau, P. Pareige, Atomic scale microstructures of high-k HfSiO thin films fabricated by magnetron sputtering, Mat. Sci. Eng. B 177 (2012) 717-720.

[19] D. Khomenkov, Y-T An, X Portier, C Labbe, F Gourbilleau, L Khomenkova, Light-Emitting and Structural Properties of Si-rich HfO_2 Thin Films Fabricated by RF Magnetron Sputtering, MRS Proc. 1617 (2013) 85-91.

[20] L. Khomenkova, M. Baran, O. Kolomys, V. Strelchuk, A.V. Kuchuk, V.P. Kladko, J. Jedrzejewski, I. Balberg, Y. Goldstein, P. Marie, F. Gourbilleau, N. Korsunska, Comparative Investigation of Structural and Optical Properties of Si-Rich Oxide Films Fabricated by Magnetron Sputtering, Adv. Mater. Res., 854 (2014) 117-124.

[21] L. Khomenkova, X. Portier, M. Carrada, C. Bonafos, B. S. Sahu, A. Slaoui, F. Gourbilleau, Ge-doped Hafnia-based Dielectrics for Non-Volatile Memory Applications, ECS Trans., 45 (2012) 331-339.

[22] D. Lehninger, L. Khomenkova, C. Röder, G. Gärtner, B. Abendroth, J. Beyer, F. Schneider, D.C. Meyer, J. Heitmann, Ge Nanostructures Embedded in ZrO2 Dielectric Films for Nonvolatile Memory Applications, ECS Trans. 66 (2015) 203-212.

[23] B.S. Sahu, F. Gloux, A. Slaoui, M. Carrada, D. Muller, J. Groenen, C. Bonafos, S. Lhostis, Effect of ion implantation energy for the synthesis of Ge nanocrystals in SiN films with HfO_2/SiO_2 stack tunnel dielectrics for memory application, Nanoscale Res. Lett., 6 (2011) 177.

[24] J.H. Choi, Y. Mao, J.P. Chang, Development of hafnium based high-k materials - A review, Mat. Sci. Eng. R 72 (2011) 97-136.

[25] J.P. Maria, D. Wicaksana, A.I. Kingon, B. Busch, H. Schulte, E. Garfunkel, T. Gustafsson, High temperature stability in lanthanum and zirconia-based gate dielectrics, J. Appl. Phys. 90 (2001) 3476-3482.

[26] M. Toledano-Luque, M. L. Lucía, A. del Prado, E. San Andrés, I. Mártil, G. González-Díaz, Appl. Phys. Lett. 91 (2007) 191502.

[27] L.-P. Feng, Z.-T. Liu, Q.-J. Liu, H. Tian, IOP Conf. Ser.: Mat. Sci. Eng. 12 (2010) 012013.

[28] D. A. Neumayer, E. Cartier, Materials characterization of ZrO_2-SiO_2 and HfO_2-SiO_2 binary oxides deposited by chemical solution deposition, J. Appl. Phys. 90 (2001) 1801-1808.

[29] C.T. Kirk, Quantitative analysis of the effect of disorder-induced mode coupling on infrared absorption in silica, Phys. Rev. B. 38 (1988) 1255-1273.

[30] P. Lange, Evidence for disorder-induced vibrational mode coupling in thin amorphous SiO_2 films, J. Appl. Phys. 66 (1989) 201-204.

[31] H. Ono, T. Ikarashi, K. Ando, T. Kitano, Infrared studies of transition layers at SiO_2/Si interface, J. Appl. Phys. 84 (1998) 6064-6069.

[32] H. García, S. Dueñas, H. Castán, A. Gómez, L. Bailón, M. Toledano-Luque, A. del Prado, I. Mártil, G. González-Díaz, J. Appl. Phys. 104 (2008) 094107.

[33] N.V. Nguyen, A.V. Davydov, D. Chandler-Horowitz, M.F. Frank, Sub-bandgap defect states in polycrystalline hafnium oxide and their suppression by admixture of silicon, Appl. Phys. Lett. 87 (2005) 192903.

[34] G. Lucovsky, J. Lüning, N.A. Stoute, H. Seo, C.L. Hinkle, B. Ju, Band Edge Traps at Spectroscopically-Detected O-Atom Vacancies in Nanocrystalline ZrO_2 and HfO_2: An Engineering Solution for Elimination of O-Atom Vacancy Defects in Non-crystalline Ternary Silicate Alloys, ECS Trans., 1(5) (2006) 381-392.

[35] K.-Ch. Lin, S.-Ch. Lee, The structural and optical properties of a-SiN_x:H prepared by plasma-enhanced chemical-vapor deposition, J. Appl. Phys. 72 (1992) 5474-5482.

[36] O. Debieu, R. Pratibha Nalini, J. Cardin, X. Portier, J. Perrière, F. Gourbilleau, Structural and optical characterization of pure Si-rich nitride thin films, Nanoscale Res. Lett., 8 (2013) 31.

Table 1. The parameters of the stacked structures investigated

Set No.	Dielectric layers (physical thickness, nm)	Estimated EOT* of tunnel dielectric, (nm)
A	12-nm-$SiN_{1.33}$ / 7-nm-HfO_2 /p-Si	1.7
B	12-nm-$SiN_{1.33}$ / 5-nm-HfO_2 / 3-nm-$SiN_{0.8}$/ p-Si	2.9
C	12-nm-$SiN_{0.8}$ / 5-nm-HfO_2 / 3-nm-$SiN_{0.8}$/ p-Si	2.9
D	12-nm-$SiN_{1.33}$ / 6-nm-$Hf_{0.27}Si_{0.05}O_{0.68}$/p-Si	1.9
E	12-nm-$SiN_{1.33}$ / 6-nm-$Hf_{0.17}Si_{0.25}O_{0.58}$/ p-Si	1.9
F	12-nm-$SiN_{1.33}$ / 4.5-nm-$Hf_{0.27}Si_{0.05}O_{0.68}$ / 3-nm-$SiN_{0.8}$ / p-Si	3.1

[*)] The EOT values for were estimated using the data for dielectric constants for Hf-based materials taken from Ref. [6,10,27]; for amorphous layers it was considered that k_{HfO2}=16, k_{HfSiOx}=12 (for Si content lower 25%), k_{SiN}=7.
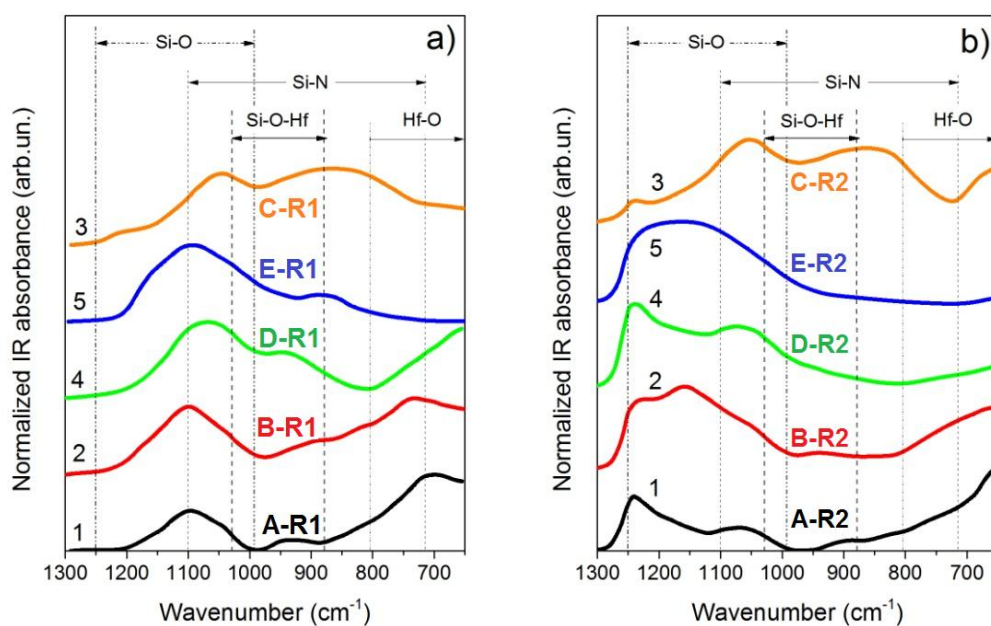
Fig.1. Normalised ATR-FTIR spectra of the samples A (1), B (2), C (3), D (4) and E (5): a) as-deposited (marked with R1) and b) annealed at 800°C for 30 s in N_2 flow (marked with R2).
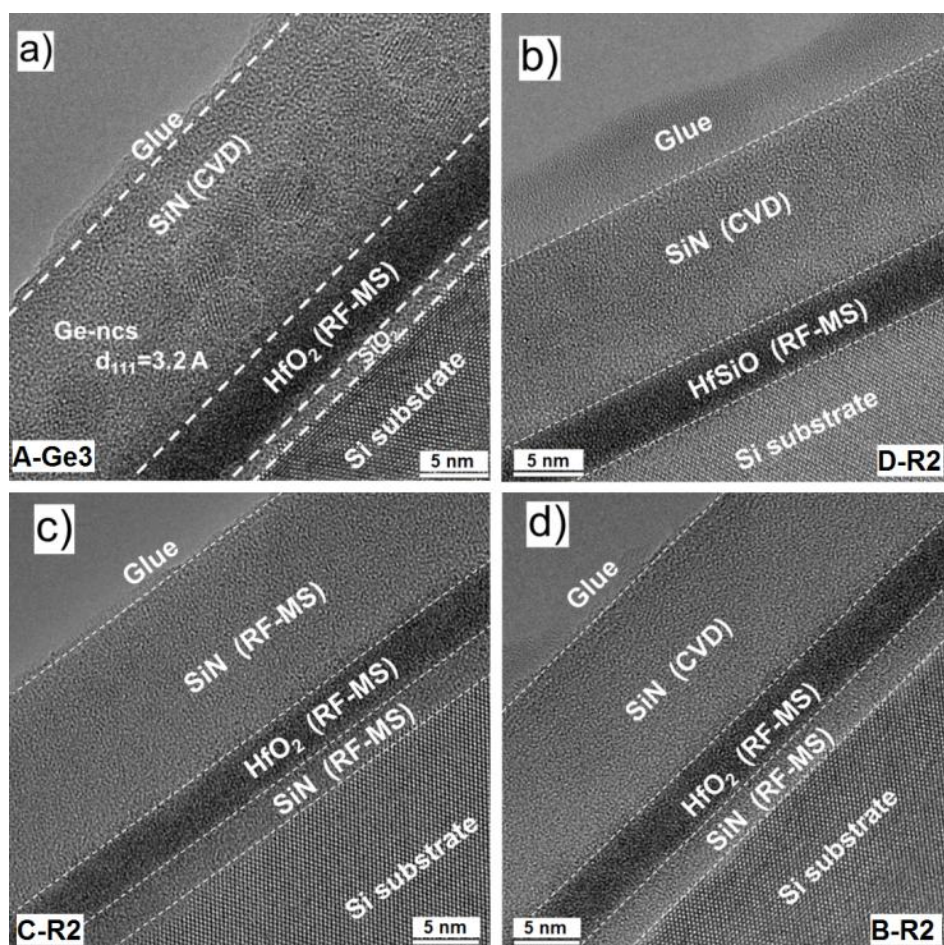
Fig. 2. High-resolution TEM bright field images of Ge-implanted (a) and not-implanted (b-d) structures: for samples A-Ge3 (a), D-R2 (b), C-R2 (c), and B-R2 (d). The samples were annealed at 800°C for 30 min in N_2 flow. Top $SiN_{1.33}$ layer was grown by PECVD (a,b,d) and RF-MS (c) approaches.
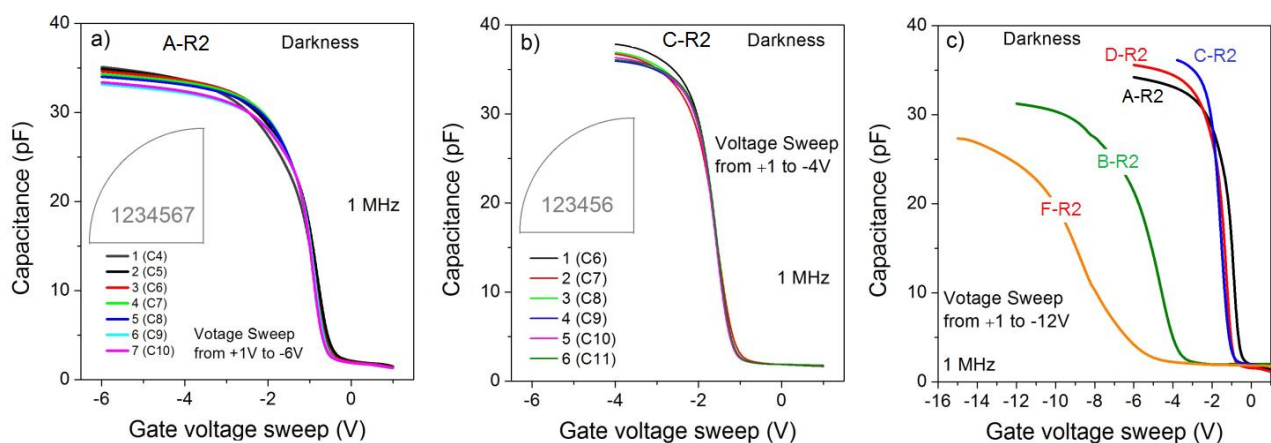
Fig.3. The single sweep C-V data for samples A-R2 (a) and C-R2 (b), demonstrated the uniformity of electrical properties. c) The comparison of single sweep C-V curves for different structures mentioned in the figure. All measurements were performed in darkness. The samples were annealed at 800°C for 30 min in N_2 flow.
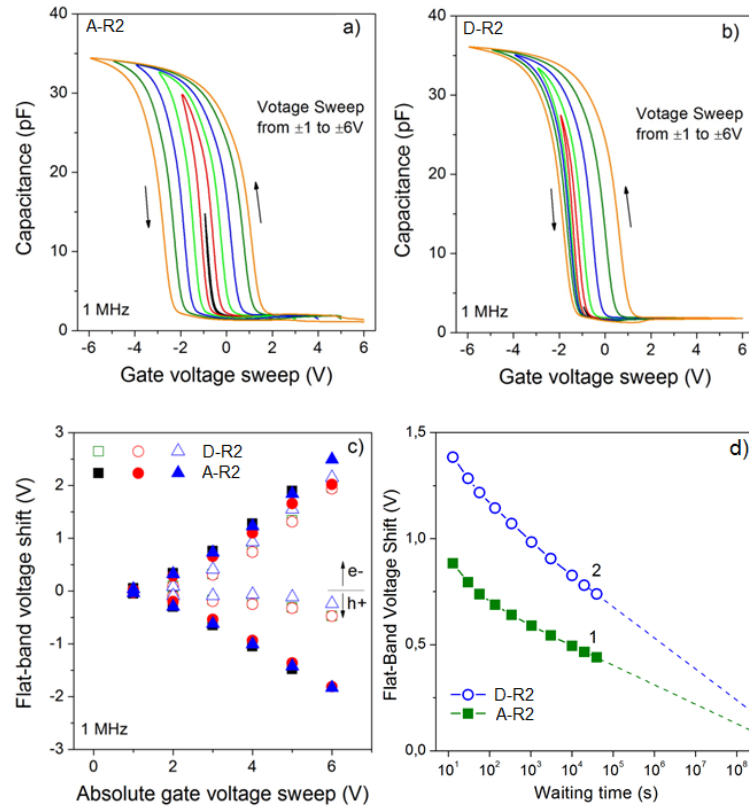
Fig.4. The C-V data for the samples A-R2 (a) and D-R2 (b). (c) Extracted flat-band voltage shift as a function of the gate voltage sweep for A-R2 and D-R2. (d) Charge retention characteristics at room temperature for the A-R2 (1) and D-R2 (2) samples after application of a gate voltage of +6V for 10s. Extrapolation curves for a 10-year waiting time are also reported. The samples were annealed at 800°C for 30 min in N_2 flow. The measurements were performed in darkness.
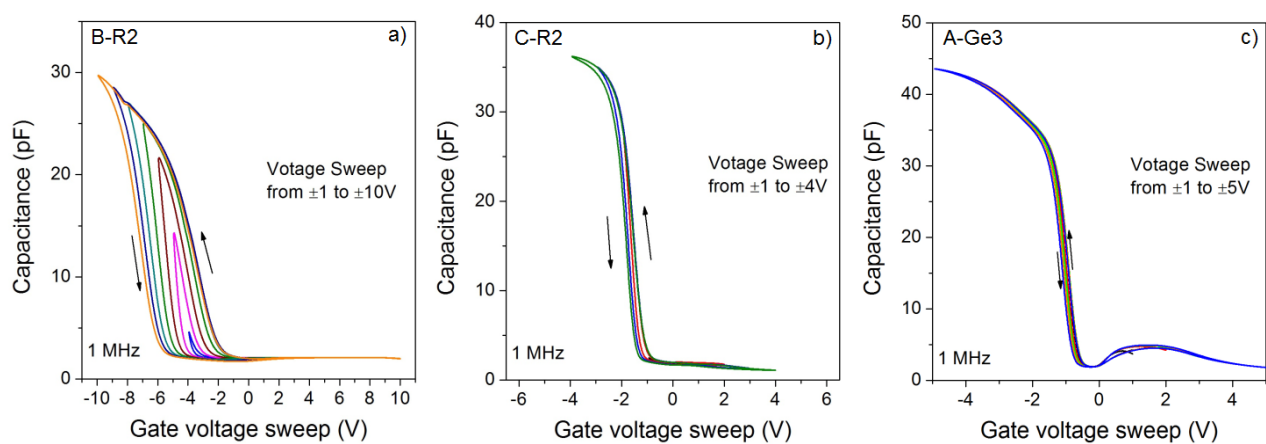
Fig.5. The C-V data for the samples C-R2 (a), B-R2 (b) and A-Ge3 (c). The samples were annealed at 800°C for 30 min in N_2 flow. The measurements were performed in darkness.

Highlights

- Stacked dielectrics were grown by magnetron sputtering and chemical vapor deposition.
- Hf-based layers were amorphous after annealing.
- The Si content affects the electrical properties of Hf-based layers.
- The Ge crystallites were formed by ion implantation and further annealing.
- The charging effect depends on the spatial distribution of Ge crystallites.